The Astronomical Journal, 158:48 (13pp), 2019 July https://doi.org/10.3847/1538-3881/ab24e4

Speckle Interferometry at SOAR in 2018

Andrei Tokovinin[1], Brian D. Mason[2], Rene A. Mendez[3], Elliott P. Horch[4,5], and Cesar Briceño[1]
[1] Cerro Tololo Inter-American Observatory, Casilla 603, La Serena, Chile; atokovinin@ctio.noao.edu, cbriceno@ctio.noao.edu
[2] U.S. Naval Observatory, 3450 Massachusetts Avenue, Washington, DC, USA; brian.d.mason@navy.mil
[3] Universidad de Chile, Casilla 36-D, Santiago, Chile; rmendez@u.uchile.cl
[4] Department of Physics, Southern Connecticut State University, 501 Crescent Street, New Haven, CT 06515, USA; horche2@southernct.edu
Received 2019 April 15; revised 2019 May 22; accepted 2019 May 24; published 2019 July 8

Abstract

The results of speckle interferometric observations at the 4.1 m Southern Astrophysical Research Telescope (SOAR) in 2018 are given, totaling 3097 measurements of 2427 resolved pairs with separations from 11 mas to 5.″9 (median 0.″15, magnitude difference up to 7 mag) and nonresolutions of 624 targets. This work continues our long-term speckle program. Its main goal is to monitor orbital motion of close binaries, including members of high-order hierarchies and *Hipparcos* pairs in the solar neighborhood. Also, pre-main-sequence stars in the Orion OB1 association were surveyed, resolving 26 out of 118 targets. In addition, we report the discovery of 35 new companions among field visual multiples (some of which are likely optical) and first-time resolutions of another 31 pairs. By combining the measurements given here with the published ones, we computed 76 orbits for the first time and updated orbital elements of 34 visual binaries. Their periods range from 0.65 to 1100 yr, and their quality varies from first tentative solutions of grade 5 to accurate elements of grades 1 and 2. Finally, a list of 53 spurious pairs discovered by various techniques and unresolved at SOAR is given.

Key words: binaries: visual

Supporting material: machine-readable tables

1. Introduction

We report here a large set of double-star measurements made at the 4.1 m Southern Astrophysical Research Telescope (SOAR) with the speckle camera, high-resolution camera (HRCam). This paper continues the series published by Tokovinin et al. (2010a, hereafter TMH10), Tokovinin et al. (2010b), Hartkopf et al. (2012), Tokovinin (2012), Tokovinin et al. (2014, 2015, 2016a), and Tokovinin et al. (2018). Most data were taken during 2018, but some older, unpublished measurements are presented here as well.

Section 2 reviews all speckle programs executed at SOAR in 2018, recent changes to the observing procedure, and the astrometric calibration. The results are presented in Section 3 in the form of electronic tables archived by the journal. We also discuss new resolutions, provide a large list of new orbital elements, and indicate likely spurious pairs. A short summary in Section 4 closes the paper.

2. Observations

2.1. Observing Programs

During 2018, HRCam (see Section 2.2) was used to execute several observing programs, some with common (overlapping) objects. Table 1 gives an overview of these programs and indicates which observations are published in the present paper. Here is a brief description of these programs.

Orbits of resolved binaries are of fundamental importance in various areas of astronomy, e.g., for direct measurement of stellar masses, binary statistics, astrometry, and objects of special interest such as binaries hosting exoplanets. Observations of tight pairs with fast motion, mostly nearby dwarfs, are prioritized at SOAR. Recently, Mason et al. (2018) published orbits of low-mass red dwarfs partially based on our data. However, classical visual binaries are also observed with appropriate temporal sampling to improve their orbits. The Sixth Catalog of Visual Binary Star Orbits, VB6 (Hartkopf et al. 2001), contains a substantial fraction of poorly determined, low-grade orbits based on inaccurate and/or sparse visual micrometric measures. This situation is slowly improving. Our work added 202 orbits to VB6, published between 2017 and 2018. More orbits are given here in Section 3.5.

Hierarchical systems of stars challenge the theories of binary-star formation. Better observational data on their statistics and architecture (orbits, relative inclinations) are needed (Tokovinin 2018b). Many hierarchies have been discovered at SOAR using HRCam, and we are following their orbital motion. An interesting class of double twins—triple systems with quasi-coplanar orbits and moderate period ratios— has been recently identified (Tokovinin 2018c). This paper adds several newly discovered hierarchies and several orbits of subsystems.

Hipparcos binaries within 200 pc are monitored with the aim of determining orbits and masses for stars in a wide range of effective temperatures and metallicities, as outlined by Horch et al. (2015, 2017, 2019). The southern part of this sample is addressed at SOAR (Mendez et al. 2017). This program overlaps with the general work on orbits. Accurate parallaxes of visual binaries, soon to be measured by *Gaia*, combined with good-quality orbits, will allow accurate measurements of stellar masses. However, it is naive to expect that *Gaia* will deliver precise parallaxes without knowledge of the orbits, as parallactic and orbital motions are coupled. The current *Gaia* data release, DR2 (Gaia Collaboration et al. 2018), contains examples of biased parallaxes of close visual pairs owing to this coupling.[6]

[5] Adjunct Astronomer, Lowell Observatory.

[6] For example, the *Hipparcos* parallax of HIP 4869, a visual binary with a period of 28 yr, is 47.3 ± 1.2 mas, matching the dynamical parallax of 44.5 mas and the *Gaia* parallax of its common proper motion companion NLTT 3509, 46.9 ± 0.1 mas. Yet, the *Gaia* DR2 parallax of 65.8 ± 0.6 mas is obviously biased, while its large error indicates the inadequacy of the current five-parameter astrometric model that does not account for the orbit.

Table 1
Observing Programs Executed with HRCam in 2018

Program	PI	N	Publ.[a]
Orbits	Mason, Tokovinin	1130	Yes
Hierarchical systems	Tokovinin	258	Yes
Hipparcos binaries	Mendez, Horch	648	Yes
Binaries in Ori OB1	Briceño	155	Yes
Kepler multi-periodic	Tokovinin, Briceño	129	Pub
Neglected binaries	R. Gould, Tokovinin	863	Yes
Young associations	Briceño, Tokovinin	227	No
Nearby K, M dwarfs	J. Winters, D. Nusdeo	100	No
Eclipsing binaries	D. Martin	34	No
TESS follow-up	C. Ziegler	90	No
Young moving groups	A. Mann	345	No
Stars with radial velocity trends	B. Pantoja	39	No

Note.
[a] This columns indicates whether the results are published here (Yes), previously (Pub), or deferred to future papers (No).

Binarity in the Orion OB1 association was studied in 2016 January (PI: C.B.) using the new catalog of pre-main-sequence (PMS) stars published by Briceño et al. (2019). Statistical analysis of this survey will be presented in a forthcoming paper. Here we provide the observational data, namely new close binaries and nonresolutions. Owing to the faintness of these targets, the laser guide star (see the instrument description in Section 2.2) was used to sharpen the images and thus increase the sensitivity at the expense of efficiency. However, the new CCD used in HRCam since 2017 has improved the magnitude limit to the point where several of these stars could be reobserved and confirmed without the help of a laser, under good seeing.

Kepler multi-periodic stars in the Upper Scorpius association were assumed to be close binaries. Indeed, we were able to resolve most of them and published our results in Tokovinin & Briceño (2018). This work raised our awareness of the poor census of binaries in this important young stellar aggregate. We continue to survey a large and nearly complete sample of PMS stars in this group and hope to publish the results soon.

Neglected binaries with small separations from the Washington Double Star Catalog (WDS; Mason et al. 2001) are observed with a low priority, as a filler. Lists of pairs in need of fresh data are provided by R. Gould (2018, private communication). A fraction of these stars are interesting because they are presently very tight, near the periastron of their orbits. Some of these pairs turned out to contain additional previously unknown components. Owing to the improved observing efficiency of the HRCam, the regular program in 2018 March–April used only part of the allocated time. Two filler programs were improvised, namely measurements of southern binaries from the WDS with separations between $0\farcs1$ and $0\farcs4$ that were never observed at SOAR and observations of wide physical pairs in search of close subsystems. These programs led to the discovery of several new hierarchical systems and helped to pinpoint a number of false pairs that pollute the WDS catalog.

Nearby K and M dwarfs were observed on request from T. Henry (PI: J. Winters and D. Nusdeo). A number of binaries were resolved, apparently for the first time.

Several programs initiated in 2018 are still in progress, such as the high-resolution follow-up of *TESS* objects of interest, the survey of stars in young moving groups, and the search for tertiary companions to low-mass eclipsing binaries.

2.2. Instrument and Observing Procedure

The observations reported here were obtained with the HRCam—a fast imager designed to work at the 4.1 m SOAR telescope (Tokovinin 2018a). The camera was mounted on the SOAR Adaptive Module (SAM; Tokovinin et al. 2016b). However, the laser guide star of SAM was not used (except in 2016 January); the deformable mirror of SAM was passively flattened and the images are seeing-limited. In most observing runs, the median image size was $\sim 0\farcs6$. The SAM module contains the atmospheric dispersion corrector. The transmission curves of the HRCam filters are given in the instrument manual.[7] We used mostly the Strömgren y filter (543/22 nm) and the near-infrared I filter (824/170 nm). A few measures were made in the V (517/84 nm) and R (596/121 nm) filters. The detector is the electron multiplication CCD iXon-888. Observations in 2016 used a different detector (Luca-DL), and the I-band response was 788/132 nm.

For each observing run, a unified observing list of objects from all programs was prepared. It contains accurate coordinates and proper motions (PMs) to allow for precise pointing of the telescope. The slews are commanded from the custom observing tool that helps to maximize the observing efficiency. When the slew angle is small, the next object is acquired almost immediately. Most observations were taken in the narrow $3''$ field with the 200×200 pixel region of interest (ROI), without binning, in the I filter; the y filter was used mostly for brighter and/or closer pairs. The pixel scale is $0\farcs01575$ and the exposure time is normally 24 ms (it is limited by the camera readout speed). Pairs wider than $\sim 1\farcs4$ are observed in a 400×400 pixel ROI, and the widest pairs are sometimes recorded with the full field of 1024 pixels ($16''$) and the 2×2 binning. The binning is used mostly for the fainter targets; it does not result in the loss of resolution in the I band, which ranges from 40 to 45 mas, depending on the magnitude and conditions. Bright stars can be resolved and measured below the formal diffraction limit (an example is given below in Section 3.5). The resolution and contrast limits of the HRCam are further discussed in TMH10 and in the previous papers of this series.

On the night of 2018 April 3/4, a total of 466 targets have been observed during 10.6 hours. The average time between targets was 1.36 min. Figure 1 illustrates the correlation between the target time and the slew distance; larger slews take a longer time. Typically, HRCam covers about 300 targets in one night.

In 2018, we implemented the automatic selection of reference stars for measuring the speckle transfer function. Their general list is based on the *Hipparcos* catalog (Perryman et al. 1997), with Hp magnitudes between 5 and 7 and excluding known binaries. For each target, the observing tool offers the five closest references from this list and points the telescope to the selected reference, if asked. In this way, there is no need to include reference stars in the observing program, and they can be chosen flexibly. Binaries with a magnitude difference of $\Delta m > 1$ mag and unresolved targets (e.g., from the binarity survey program) are used as reference during data

[7] http://www.ctio.noao.edu/soar/sites/default/files/SAM/-archive/hrcaminst.pdf

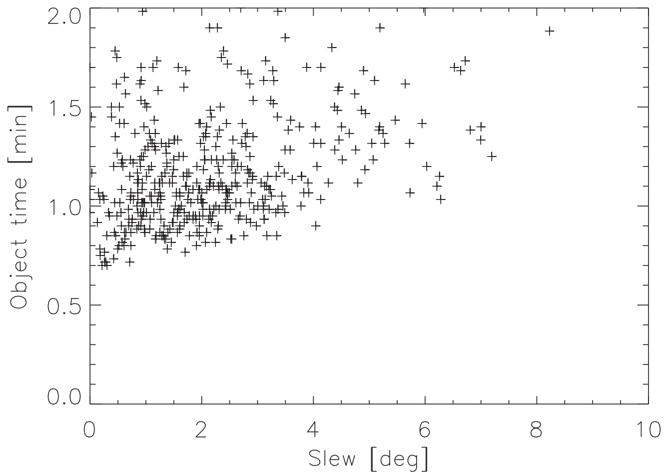

Figure 1. Correlation between observing time per object and the slew distance for the night of 2018 April 3/4. The vertical axis plots time between observations of successive objects.

processing (see Tokovinin 2016a), so special observations of reference stars are needed only occasionally.

The first observations reported here were obtained in 2017 December, and the last in 2018 December. HRCam was used during scheduled observing runs, but also in parts of engineering nights available from other work. Figure 2 plots the cumulative number of observations executed during this year, which reaches almost 5000. The largest number of objects was covered during four scheduled nights in 2018 March–April.

2.3. Data Processing and Calibration

The data processing is described in TMH10 and Tokovinin (2018a). We use the standard speckle interferometry technique based on the calculation of the power spectrum and the speckle autocorrelation function (ACF) derived from it. Companions are detected as secondary peaks in the ACF and/or as fringes in the power spectrum. Parameters of the binary and triple stars (separation ρ, position angle θ, and magnitude difference Δm) are determined by modeling the observed power spectrum. Additionally, the true quadrant is found from the shift-and-add images, whenever possible.

The pixel scale and angular offset are determined by observations of several relatively wide calibration binaries. Their motion is modeled based on previous observations at SOAR, with individual scale and orientation corrections for each observing run. The models are adjusted iteratively. The latest adjustment of 65 calibrators was done in 2017 November. Typical rms deviations of observations from these models are $0\overset{\circ}{.}2$ in angle and 1 to 3 mas in separation.

The adopted calibration procedure assures good internal consistency of the SOAR speckle astrometry but does not preclude the existence of global systematic errors. We compared a subset of 21 calibrators to the *Gaia* astrometry provided in the DR2 (Gaia Collaboration et al. 2018). The separations range from $0\overset{''}{.}82$ to $2\overset{''}{.}2$ (the remaining calibrators are not resolved in the DR2). We computed the *Gaia* position angles and separations for J2000 from the coordinates, corrected them for precession in angle to the epoch of 2015.5, and compared to the positions predicted by our models for the same date.

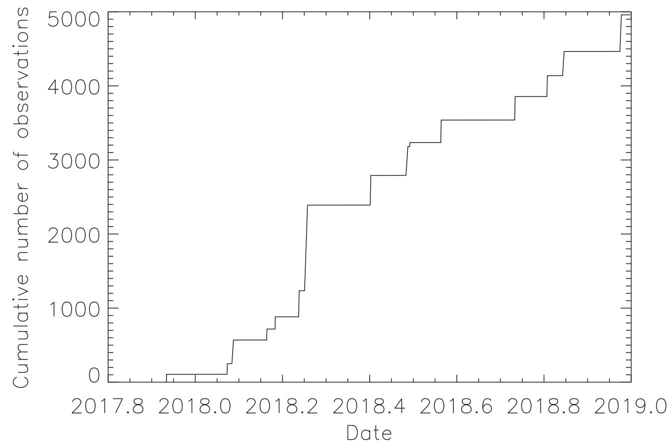

Figure 2. Cumulative plot of the number of HRcam observations at SOAR during 2018 (all programs).

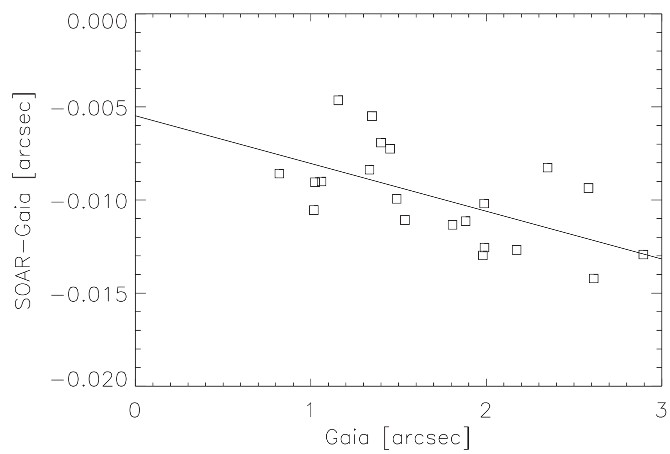

Figure 3. Comparison between SOAR and *Gaia* separations of calibration binaries. The line is a linear fit given by Equation (1).

The comparison reveals a small but measurable difference between the SOAR and *Gaia* systems. The position angles $\theta_{\rm SOAR}$ have, on average, an offset of $-0\overset{\circ}{.}17$, with an rms scatter of $0\overset{\circ}{.}12$ around this value (or 3.1 mas in the tangential direction). The scatter decreases with separation. The SOAR separations are smaller compared to those from *Gaia*, and a linear trend is found:

$$\rho_{\rm SOAR} - \rho_{Gaia} \approx -0.0054 - 0.0025\rho_{Gaia}, \tag{1}$$

as shown in Figure 3. The rms scatter around this line is 2.05 mas.

The systematical errors of the HRCam astrometry are less than the declared calibration accuracy, 0.5% in scale and $0\overset{\circ}{.}5$ in angle. We do not apply these corrections to the data presented here but rather prefer to keep the HRCam astrometry on the same system for consistency. When the *Gaia* DR4 containing a large volume of double-star astrometry becomes available, we will repeat and extend its comparison with the HRCam and will determine the final corrections. At present, it cannot be excluded that the trend seen in Figure 3 is not caused, at least partially, by errors in the *Gaia* data. The optics of the HRcam has a cubic distortion that reduces the pixel scale off-axis. However, this distortion is very small: the relative pixel scale is reduced only by 3×10^{-5} for a $4''$ offset.

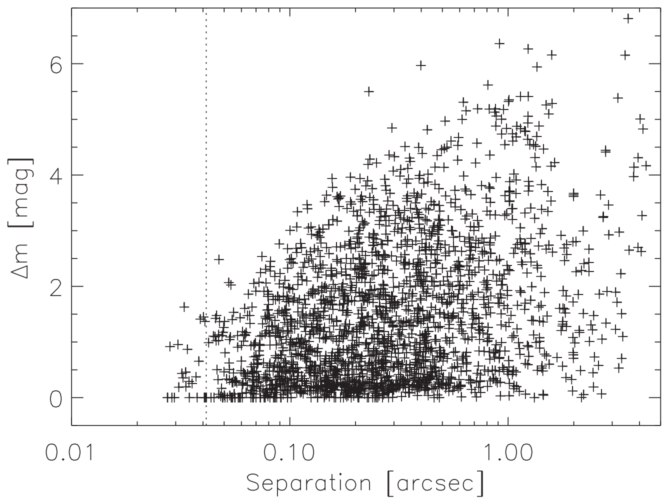

Figure 4. Magnitude difference in the *I* band vs. separation for pairs resolved in this filter. The vertical dotted line marks the formal diffraction limit of 41 mas.

3. Results

3.1. Data Tables

The results (measures of resolved pairs and nonresolutions) are presented in almost the same format as in the previous papers of this series. The long tables are published electronically; here we describe their content. To illustrate the resolution and dynamic range of this data set, we plot in Figure 4 the magnitude difference versus separation for pairs resolved in the *I* filter.

Table 2 lists 3097 measures of 2427 resolved pairs and subsystems, including the new discoveries. The pairs are identified by their WDS codes and discoverer designations adopted in the WDS catalog (Mason et al. 2001), as well as by alternative names in column (3), mostly from the *Hipparcos* catalog. Equatorial coordinates for the epoch J2000 in degrees are given in columns (4) and (5) to facilitate matching with other catalogs and databases. In the case of multiple systems, the position measurements and their errors (columns 9–12) and magnitude differences (column 13) refer to the individual pairings between components, not to their photocenters. As in the previous papers of this series, we list the internal errors derived from the power spectrum model and from the difference between the measures obtained from two data cubes. The median internal error is 0.3 mas, and 95% of these errors are less than 3 mas. The real external errors are usually larger, especially for difficult pairs with substantial Δm and/or with small separations. Residuals from orbits (Section 3.5) and from the models of calibrators, typically between 1 and 5 mas rms, characterize the external errors of the HRcam astrometry.

The flags in column (14) indicate cases when the true quadrant is determined (otherwise the position angle is measured modulo 180°), when the photometry of wide pairs is derived from the long-exposure images (this reduces the bias caused by speckle anisoplanatism) and when the data are noisy or the resolutions are tentative. The exact definition of noisy data, related to the signal-to-noise ratio in the power spectrum, is given in TMH10; such observations have a lower resolution limit and precision. For pairs wider than $\sim 1''$, our estimates of Δm may be too large owing to anisoplanatism and potential truncation of the companion's image in the narrow $3''$ field.

Table 2
Measurements of Double Stars at SOAR

Col.	Label	Format	Description, Units
1	WDS	A10	WDS code (J2000)
2	Disc.	A16	Discoverer code
3	Other	A12	Alternative name
4	R.A.	F8.4	R.A. J2000 (deg)
5	Decl.	F8.4	decl. J2000 (deg)
6	Epoch	F9.4	Julian year (yr)
7	Filt.	A2	Filter
8	N	I2	Number of averaged cubes
9	θ	F8.1	Position angle (deg)
10	$\rho\sigma_\theta$	F5.1	Tangential error (mas)
11	ρ	F8.4	Separation (arcsec)
12	σ_ρ	F5.1	Radial error (mas)
13	Δm	F7.1	Magnitude difference (mag)
14	Flag	A1	Flag of magnitude difference[a]
15	$(O-C)_\theta$	F8.1	Residual in angle (deg)
16	$(O-C)_\rho$	F8.3	Residual in separation (arcsec)
17	Ref.	A8	Orbit reference[b]

Notes.
[a] Flags: q, the quadrant is determined; *, Δm and quadrant from average image; :, noisy data.
[b] References to VB6 are provided at http://ad.usno.navy.mil/wds/orb6/wdsref.txt; Table 7 refers to Table 7 of this paper.

(This table is available in its entirety in machine-readable form.)

Table 3
Unresolved Stars

Col.	Label	Format	Description, Units
1	WDS	A10	WDS code (J2000)
2	Disk.	A16	Discoverer code
3	Other	A12	Alternative name
4	R.A.	F8.4	R.A. J2000 (deg)
5	Decl.	F8.4	decl. J2000 (deg)
6	Epoch	F9.4	Julian year (yr)
7	Filt.	A2	Filter
8	N	I2	Number of averaged cubes
9	$\rho_{\min}$	F7.3	Angular resolution (arcsec)
10	$\Delta m(0.15)$	F7.2	Max. Δm at $0\farcs15$ (mag)
11	$\Delta m(1)$	F7.2	Max. Δm at $1''$ (mag)

(This table is available in its entirety in machine-readable form.)

For binary stars with known orbits, the residuals to the latest orbit and its reference are provided in columns (15)–(17). The orbits computed in this paper are referenced as “Tab. 7.”

Nonresolutions are reported in Table 3. Columns (1) to (8) have the same meaning and format as in Table 2. Column (9) gives the minimum resolvable separation when pairs with $\Delta m < 1$ mag are detectable. It is computed from the maximum spatial frequency of the useful signal in the power spectrum and is normally close to the formal diffraction limit λ/D. Columns (10) and (11) provide the indicative dynamic range, i.e., the maximum magnitude difference at separations of $0\farcs15$ and $1''$, respectively.

Table 2 contains about a hundred pairs resolved for the first time; some of those were confirmed in subsequent observing runs. Almost as many additional first resolutions belonging to the projects led by other PIs will be reported elsewhere (these pairs are not published here), while 54 new pairs in Upper

Scorpius are published by Tokovinin & Briceño (2018). In the following subsections, we discuss new resolutions in the context of observing programs.

3.2. New Pairs in Orion OB1

In 2016 January 16–18, we surveyed young low-mass stars in the Orion OB1 association. We targeted 150 objects among the brightest ($V \leqslant 15$) of the 2062 T Tauri stars (TTS) reported by Briceño et al. (2019). This sample includes 74 young stars in the ∼5 Myr old OB1b subassociation and another 74 in the older OB1a subassociation; the latter are distributed as follows: 42 are part of the widely distributed young field population of OB1a (∼11 Myr), 17 are members of the 25 Ori cluster, 8 of the HD 35762 cluster (both ∼8 Myr old), and 7 belong to the HR 1833 cluster (∼13 Myr). There are 30 accreting classical TTS (CTTS) stars among the sample, 111 nonaccreting weak-line TTS (WTTS) and 7 of the newly-defined C/W class, objects with accretion properties intermediate between CTTS and WTTS, possibly because they are in the process of ending their accretion phase. Roughly half of the CTTS are located in OB1b. This is by design, in order to have a similar number of accreting TTS in both of the regions for statistical comparison of multiplicity of accreting and nonaccreting stars. In reality, the younger OB1b region contains roughly twice as many CTTS as the older OB1a (which includes the three clusters mentioned above).

As most targets were quite faint, we used the SAM laser guide star for partial compensation of turbulence to get sharper images. The adaptive optics (AO) loop did not compensate for the tilts; instead, the individual frames were centered and co-added in the data processing. The good seeing during these observations and the AO compensation resulted in the median FWHM of recentered images of $0\farcs33$ (best $0\farcs25$), while the site monitor reported seeing from $0\farcs5$ to $1''$ during these observations. In the morning, when Orion was too low, we observed stars in the young association ϵ Chamaeleontis (Briceño & Tokovinin 2017).

Data cubes were taken with the HRCam in the I filter (response 788/132 nm for the Luca DL camera used in 2016) with an exposure time of 0.1 or 0.2 s per frame, longer than usual, and with the 2 × 2 binning. Data cubes with a smaller field and shorter exposures were also acquired; they were useful for stars brighter than $I = 12$ mag. The data were processed by the standard speckle pipeline. In addition, we examined average recentered images (Figure 5) where the smooth component approximated by the Moffat function was subtracted. This helped to detect or confirm faint companions at larger separations. In 2017 and 2018, some newly discovered close binaries were remeasured without the laser image sharpening because the HRCam used a new CCD camera with better sensitivity.

Statistical analysis of the binary population in the Ori OB1 association is beyond the scope of this paper. It will use seeing-limited images and *Gaia* astrometry to address wider binaries. Here we only report the speckle results. The PMS stars in Ori OB1 are identified by their CVSO numbers from Briceño et al. (2019) in the main tables. A summary of 26 new pairs discovered in 2016.04 in Ori OB1 is given in Table 4. It contains the WDS code derived from the J2000 coordinates (naturally, these objects are not yet present in the actual WDS), CVSO number, separation, angle, and magnitude difference in the I band. An asterisk in the last column indicates subsequent confirmation in 2017–2018. Interestingly, the closest pair CVSO 141 shows some orbital motion in two years. The number of observed CVSO stars (including nonresolutions) is 118. During a period of poor seeing we also observed brighter stars in Orion and resolved J05271+0351 (HIP 25493). The number of observations for this program (counting repeated measurements) is 155.

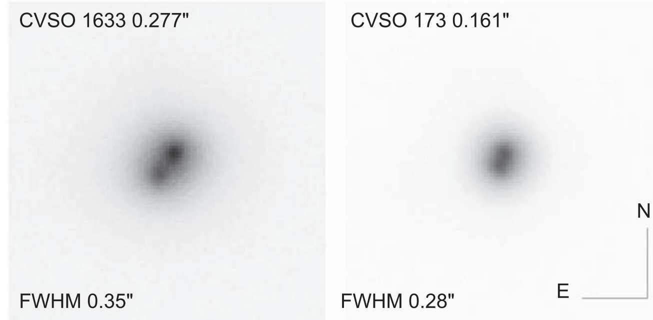

Figure 5. Centered images of two newly resolved close binaries in Orion OB1, displayed on an arbitrary negative scale. The binary separation and FWHM resolution are indicated.

Table 4
New Pairs in Orion OB1

WDS	CVSO	ρ (arcsec)	θ (deg)	ΔI (mag)	Conf.
05022−0408	267	0.312	328.6	1.3	
05042−0005	271	1.102	119.6	2.8	
05067−0318	286	1.257	251.6	4.5	
05119−0157	324	0.675	66.1	3.6	*
05204−0001	7	0.188	205.4	1.5	*
05220+0144	516	0.179	276.4	1.5	*
05223+0201	530	0.295	229.9	0.6	*
05245+0148	2001	0.640	95.8	4.1	
05253−0158	33	2.122	46.4	4.6	
05257+0145	35	1.283	272.7	2.0	
05261−0209	840	0.187	198.2	0.6	*
05277+0312	985	0.684	285.7	2.2	
05294+0136	1169	0.563	279.3	1.0	
05296−0135	65	1.502	152.6	0.7	
05318−0155	98	0.165	298.5	1.8	*
05319−0045	1328	0.572	309.0	0.7	
05335−0132	120	3.720	314.2	2.0	
05342−0009	130	1.269	106.5	1.8	
05345−0204	1506	2.469	32.1	3.7	
05352−0043	1577	0.185	267.7	3.4	*
05353−0050	141	0.086	68.9	0.0	*
05356−0143	1620	0.458	135.1	2.6	
05357+0021	1633	0.278	143.4	0.6	*
05375−0048	155	1.981	128.6	1.1	
05379−0009	1789	1.510	225.2	1.5	
05397−0035	173	0.161	157.4	0.3	*

3.3. New Multiple Systems

As in the previous papers of this series, we report discoveries of new visual multiple systems containing three or more resolved components. This information is ingested into the current version of the multiple-star catalog (MSC; Tokovinin 2018b). Although the high angular resolution of HRCam helps to discover inner close pairs in known binaries, its high dynamic range has also enabled detection of 11 faint

Table 5
New Visual Multiple Systems

WDS	Outer	ρ_{out} (arcsec)	Inner	ρ_{in} (arcsec)
03056−2328	RST 2294 AC*	1.31	AB	0.60
03338−1508	TOK 239 AB	625	Ba, Bb*	0.93
05441−1934	HDS 766 AC*	1.23	AB	0.07
07435+0329	STF 1134 AB	9.6	Ba, Bb*	0.05
08143−5444	RST 3579 AB	0.38	Aa, Ab*	0.04
08159−3056	BU 454 AB	1.86	Ba, Bb*	0.35
08198−7131	BSO 17 AB	63.8	Aa, Ab*	1.34
08297−6708	HDS 1215 AC*	0.97	Aa, Ab	0.13
08429−7707	HDS1253 AB	0.21	Aa, Ab*	0.09
08515−8018	LDS 244 AB	37.0	Aa, Ab*	0.87
08540+0825	STT 195 AB	13.7	Aa, Ab*	0.08
09033−7036	HEI 223 AC*	0.46	AB	0.07
09173−6841	I 358 AB,C	18.8	Ca, Cb*	0.56
09180−5453	JNN 69 AB	0.52	Aa, Ab*	0.05
10268−6254	HDS 1501 AB	4.0	Ba, Bb*	0.09
11000−3507	HIP 53776AB*	0.65	BC*	0.11
11155−6725	HDS 1605 AC	2.65	Aa, Ab*	0.51
11470−6545	LDS 365 AB	16.4	Aa, Ab*	0.23
12197+0533	A 1597 AC*	1.42	AB	0.67
13044−1316	HU 642 AC*	1.57	AB	0.50
13114+0938	LDS 5771 AB	81.8	Aa, Ab*	0.52
13343−1132	HDS 470 AB	3.76	BC*	0.79
13343−1132	HDS 470 BC*	0.79	Ca, Cb*	0.13
14139−3203	SEE 201 AB	17.4	Aa, Ab*	0.97
14243−6223	RST 4525 AB	0.49	BC*	0.07
15386−5128	RST 2970 AC*	0.88	AB	0.39
15432+1340	BU 619 AB	0.65	BC*	0.25
15495+2528	WSI 111 AC*	0.51	Aa, Ab	0.20
15549−3731	B 852 AB	0.99	BC*	0.18
16087−2523	JNN 221 AB	0.82	Aa, Ab*	0.05
16439−3234	JSP 696 AC*	0.93	AB	0.27
16509−1950	B 1830 AB	0.39	BC*	0.05
16545−2734	B 322 AC*	1.27	AB	0.21
18321−4046	RST 4014 AB	0.27	Aa, Ab*	0.06
19243+2032	HDS 2752 AC*	0.98	AB	0.27
19251−2303	RST 3225 AB	1.24	Aa, Ab*	0.17

outer companions to known binaries. In HIP 53776, both inner and outer pairs are new discoveries. In 13343−1132, the newly discovered component C is itself a close pair, Ca,Cb. Resolution of the secondary component in 06401−3033 was reported by Elliott et al. (2015), but not reflected in the WDS, so this triple system is reobserved here.

Table 5 presents 35 new multiple systems in compact form. Its first column gives the WDS code. Column (2) gives the discoverer code and the components' designation of the outer pair are given, followed by the separation in arcseconds in column (3). Then in columns (4) and (5) the same data are given for the inner subsystem. New subsystems (either outer or inner) are distinguished by an asterisk. Many close inner pairs have short estimated periods, favoring determination of their orbits within a few years, like the nearby low-mass hierarchies 09180−5453 and 10268−6254.

In several triple systems presented here the projected outer and inner separations are comparable (Figure 6). If these pairs are physical and the true three-dimensional separations are also comparable, the inner and outer orbits strongly interact with each other. Further monitoring will help to investigate the dynamics of these systems and, of course, to confirm or refute the physical nature of the companions. From this perspective,

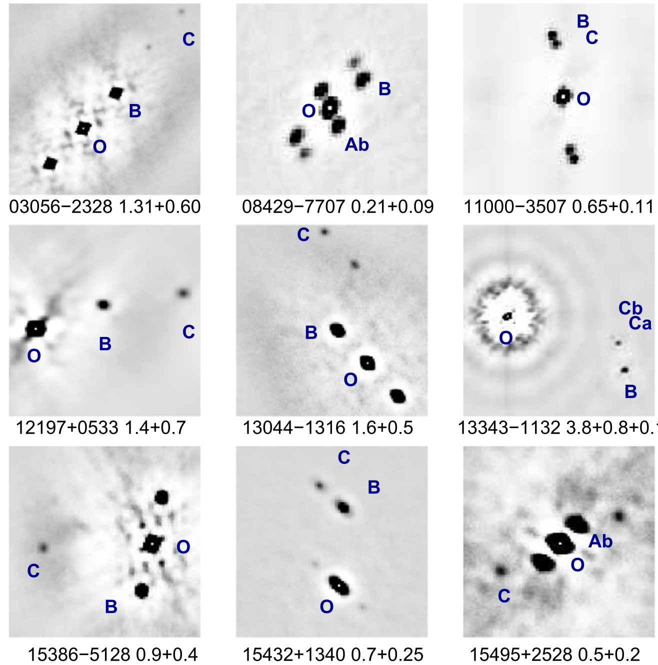

Figure 6. Fragments of ACFs of new triple systems with comparable separations between components (trapezia). North is up, east is left, and the scale is arbitrary. The WDS code and separations in arcseconds are given below each fragment. The peaks corresponding to the locations of the components are indicated by letters; other peaks are their symmetric counterparts and the cross-correlations between the two secondaries (an ACF of a triple star contains 6 peaks). The central peak of the ACF is marked by the white dot and the letter O.

nearby systems with fast relative motion will be most interesting. On the contrary, a faint tertiary companion to a distant star with a slow PM in a crowded region of the sky is likely optical. Such is the case of 08297−6708, 15386−5128, 16439−3234, and 16545−2734. The new component C in 05441−1934 with $\Delta I \sim 5$ mag is found in the *Gaia* DR2 at a slightly different position, so it is likely optical, despite the low crowding. The tertiary in 13044−1316 is likely physical because it keeps the same position in DR2 while the PM is fast. Therefore, this triple could be a genuine trapezium. The status of other new tertiaries remains unknown.

3.4. New Binaries

In Table 6 we list 31 first-time resolutions of binaries. Some of them could have been spotted by other observers but are not yet published and listed in the WDS, being "new" in this sense. The columns give the WDS code, alternative name, separation, magnitude difference, and the observing program code, where EH refers to the list of objects provided by E.H. (all these stars were resolved at the WIYN telescope in 2012–2013), HIP is the survey of *Hipparcos* stars, and SB2 marks double-lined spectroscopic binaries. Four pairs are serendipitous resolutions of reference stars (code Ref). The $0\farcs6$ pair TDS8647CD (13012−4109) belonging to the visual multiple system (code MSC) is proven here to be spurious, like many other similar *Tycho* binaries (Tokovinin et al. 2018), but we resolved instead a different pair. HIP 25493 was observed as part of the Orion OB1 survey.

Table 6
New Double Stars

WDS	Name	ρ (arcsec)	Δm (mag)	Program[a]
01244−2803	HIP 6566	1.01	3.7	EH
01384−1552	HIP 7639	0.51	5.0	EH
03030−0205	HIP 14194B	0.04	0.0	SB2
05066−7734	HIP 23776	0.06	0.5	HIP
05271+0351	HIP 25493	0.88	5.1	Ori
07292+1246	HIP 36371	0.36	3.2	Ref
11367−0919	HIP 56631	0.14	2.6	EH
12120+0520	HIP 59479	0.08	0.0	EH
12213−3033	HIP 60252	0.47	4.4	HIP
12215+0749	HIP 60272	0.53	3.2	EH
12532+2859	HIP 62881	0.10	0.2	EH
12578+2252	HIP 63262	1.32	3.2	EH
13012−4109	TDS8647CD?	0.28	3.7	MSC
15555−2616	HIP 77984	0.83	3.8	Ref
16368+0422	HIP 81351	1.25	3.8	EH
17111−2039	HIP 84056	1.08	4.9	Ref
17293−3839	HIP 85583	1.63	4.2	HIP
17340−1750	HIP 85952	0.81	5.6	HIP
17463−4044	HIP 86965	0.21	2.9	HIP
17511+2704	HIP 87375	0.42	3.2	EH
17531−7501	HIP 87539	0.25	1.9	HIP
18203−3526	HIP 89589	0.12	3.0	Ref
18255−1439	HIP 90299	0.20	0.9	HIP, EH
18393−3742	HIP 91471	0.22	2.4	HIP
18432−5730	HIP 91808	0.06	0.0	HIP
19242−6260	HIP 95385	0.08	1.2	HIP
19345+1759	HIP 96268	0.07	0.9	EH
19476+0105	ENG 67Aa, Ab	0.62	5.0	HIP
20446+1333	HIP 102380	1.54	5.1	EH
21017−4431	HIP 103776	0.45	0.8	HIP
22261−1248	HIP 110741	0.73	3.1	EH

Note.
[a] EH, pair resolved previously by E.H. at the WIYN telescope; HIP, *Hipparcos* binary; SB2, double-lined spectroscopic binary; Ref, reference star; Ori, member of Orion OB1 association; MSC, multiple system.

3.5. New and Updated Orbits

Long periods of classical visual binaries and slow accumulation of measures have established the tradition of computing tentative orbits as soon as feasible. As a result, the VB6 catalog (Hartkopf et al. 2001) contains a large number of provisional, low-quality orbits. Naturally, the orbits are improved (or drastically revised) in response to new measures, so that the orbit calculation becomes an almost continuous process. In theory, it could be automated. In practice, however, critical evaluation and proper weighting of the data (especially the historic visual measures) is essential. Different authors have different schemes and approaches in this matter. We adopt weights proportional to σ^{-2}, where the errors σ are assigned according to the measurement technique (e.g., from 2 to 5 mas for speckle interferometry at 4 m class telescopes, 10 mas for *Hipparcos*, 50 mas or larger for visual micrometer measures) and corrected iteratively to reduce the impact of outliers, if necessary. The IDL program `ORBIT` is used (Tokovinin 2016b).

Our speckle program at SOAR has contributed to the improvement of existing orbits and the determination of new orbits, especially for the close *Hipparcos* and interferometric pairs. During 2017 and 2018, more than 200 orbits based on the SOAR data were added to the VB6 catalog. Here we provide additional 110 orbits in Table 7. Provisional grades and references to previous orbits are given in the last columns; asterisks mark orbits where radial velocities from the literature are used jointly with position measures. For provisional orbits of grade 5, we do not list the formal errors, which are large and misleading when the observations do not constrain all orbital elements and we fix some of them. Although provisional orbits are poorly constrained, their publication helps to plan further observations of fast binaries like 04400−3105 (period 14 yr) and to model the motion of long-period pairs, where no substantial orbit improvement is expected in the coming decades. For circular and/or face-on orbits, some Campbell elements become degenerate and they are fixed accordingly.

As an example of a fast binary from our *Hipparcos* program, we show in Figure 7 the first orbit of HIP 6626 (HDS 184, GJ 1083), a K7V dwarf within 25 pc from the Sun. Measurements at SOAR taken during four years, together with the first *Hipparcos* resolution, define the orbit quite well. The short period of 6.3 yr implies a large radial velocity (RV) amplitude. Realizing this, we took one spectrum with CHIRON on 2018.916 and, indeed, detected the double lines with an RV difference of 20 km s^{-1}. Further monitoring and accurate parallax from future *Gaia* data releases will lead to precise mass measurements of these stars.

Figure 8 illustrates a particularly difficult case of orbit calculation. The 4th magnitude star α Volantis (HR 3615, HD 78045, HIP 4438, spectral type kA3hA5mA5V) has been resolved at SOAR in 2010 at 29 mas and later measured 17 times at similar separations or unresolved. It was placed on the observing program on request by J. Patience, as part of the survey of Herbig AeBe stars. With the small separation, small $\Delta y = 0.2$ mag, and frequent nonresolutions, it was difficult to make sense of the available measures. In the beginning of 2018, a provisional orbit with a one-year period was computed. To test it, the star was observed in 2018.5, outside its normal visibility season. This critical observation invalidated the proposed orbit, but helped to establish the true orbital period of 0.6515 $\pm$ 0.001 yr (238 days). All measures were examined and reprocessed where necessary, reaching below the nominal diffraction limit of 30 mas and down-weighting the data affected by telescope vibration. The weighted rms residuals to the orbit are 1.5 mas in both coordinates. With the *Gaia* DR2 parallax of 26.49 mas, the mass sum is 4.2 solar. Based on its kinematics, the star may belong to the 300-Myr-old UMa moving group.

Several binaries in Table 7 have subsolar metallicity. For example, HIP 24076 (05103−0736, A 484) with [Fe/H] = −0.57 dex (Holmberg et al. 2009) goes through the periastron of its eccentric orbit in 2019.0 and is being followed both by speckle and by spectroscopy. Accurate orbits and masses will be used to test stellar models, continuing the work of Horch et al. (2019) on metal-poor stars.

3.6. Spurious Double Stars

A star is considered to be double if it was resolved at least once. If the resolution was spurious, as shown by subsequent observations, the double-star label still persists. It is difficult to prove that a given star is *not double* because its nonresolutions can be explained by the orbital motion that brings the components too close together, by a large Δm, or by poor observing conditions. The WDS records only the last measure, so, when a given pair was repeatedly unconfirmed, this fact is

Table 7
Visual Orbits

WDS *HIP*	Disc.	P (yr)	T (yr)	e	a (arcsec)	Ω (deg)	ω (deg)	i (deg)	Grade	Ref.[a]
00008+1659	BAG 18	66.62	1990.25	0.372	0.531	142.2	−1.1	192.3	5	New
00569−5153	B 1418	19.82	2015.44	0.404	0.227	279.8	323.3	85.8	3	New
4448		±0.54	±0.20	±0.054	±0.012	±0.5	±7.3	±0.6		
01205−1957	TOK 203	8.53	2013.99	0.627	0.284	108.8	106.3	104.0	3	Gln2006
6273		±0.37	±0.13	±0.044	±0.016	±2.0	±2.5	±1.9		
01250−3251	HDS 184	6.313	2018.549	0.515	0.1445	107.4	165.8	73.9	3	New
6626		±0.065	±0.021	±0.007	±0.0010	±0.5	±2.1	±0.8		
02166−5026	TOK 185	11.29	2014.17	0.066	0.090	270.4	31.8	45.3	2	Tok2017b
10611		±0.46	±0.36	±0.031	±0.002	±4.8	±10.7	±1.9		
02254+0135	HDS 315	600	2002.5	0.64	0.674	63.4	237.4	50.0	5	New
02336−3910	B 674	327.8	2027.35	0.68	0.238	36.8	150.1	172.0	5	New
03014+0615	HDS 385	14.893	2013.111	0.419	0.1169	161.4	195.5	54.3	1	Tok2015c
14075		±0.042	±0.055	±0.005	±0.0011	±0.9	±1.8	±0.7		
03193−5053	RST 70	51.1	2017.33	0.74	0.176	44.7	67.8	52.8	4	New
15451		±2.7	±0.29	±0.08	±0.025	±19.1	±12.9	±7.8		
03305+2006	RAO 11 Ba, Bb	31.46	2015.18	0.395	0.294	63.0	18.8	103.1	3	New*
16329		±0.25	±0.37	±0.019	±0.024	±4.4	±5.4	±1.6		
03363−1728	HDS 456	21.00	2018.05	0.841	0.107	92.8	197.9	134.3	2	New
16803		±0.27	±0.08	±0.008	±0.003	±5.9	±8.2	±2.4		
04028−3115	HDS 511	84.50	2020.83	0.293	0.207	174.9	258.6	117.4	5	New
04302−1747	B 1937	111.55	1908.67	0.160	0.213	123.4	0.0	180.0	5	Zir2008
04312+0157	HDS 585	65.1	2014.30	0.422	0.370	259.9	170.2	76.1	3	New
21092		±4.5	±0.28	±0.025	±0.013	±0.7	±2.5	±0.7		
04375+1509	CHR 153	127.7	2047.35	0.251	0.712	144.6	75.1	74.9	5	New
04400−3105	HDS 602	14.0	1995.58	0.700	0.176	108.2	75.3	139.0	5	New
04518+1339	BU 552 AB	97.7	1982.193	0.592	0.7432	142.6	312.3	50.3	2	Sod1999
22607		±1.4	±0.054	±0.003	±0.0066	±0.6	±0.4	±0.3		
05048+1319	HEI 104	140	2034.124	0.420	0.160	182.4	139.9	84.6	5	New
05103−0736	A 484	18.936	2000.147	0.787	0.1555	111.5	309.9	106.4	2	Tok2017b*
24076		±0.064	±0.065	±0.005	±0.0019	±0.5	±0.9	±0.5		
05267−6436	I 1150	907	2020.71	0.822	0.722	171.5	212.0	55.5	5	New
05334−4923	HDS 732 Aa, Ab	21.9	2020.609	0.850	0.162	313.1	245.2	76.0	4	New
26050		±1.2	±1.445	fixed	±0.037	±15.0	±4.9	±6.9		
05427−6708	I 745	208	2017.19	0.775	0.568	238.3	205.8	72.1	4	New
26904		±33	±0.29	±0.021	±0.051	±2.2	±2.4	±1.4		
05505−0310	HDS 785	105.6	2021.9	0.65	0.208	170.2	147.9	118.0	5	New
05590−0740	HDS 809	100	216.13	0.314	0.457	29.9	129.9	31.5	5	New
06023+0142	CHR 162	200	2033.556	0.88	0.3242	219.4	238.2	102.8	5	New
06143−1729	A 3025	226	2016.09	0.850	0.588	94.9	128.7	154.7	4	New
29601		±17	±0.04	±0.008	±0.027	±11.6	±13.0	±4.8		
06201−0752	HDS 866	58.23	2023.03	0.66	0.186	82.6	243.7	81.4	5	New
06314+0749	A 2817	31.71	2015.333	0.290	0.1943	55.2	142.0	38.4	1	Tok2015c
31089		±0.19	±0.075	±0.004	±0.0012	±1.4	±2.3	±0.9		
06510+0551	HDS 950	30.5	2016.59	0.718	0.106	165.9	242.4	134.5	5	New
06533−1902	CHR 169	37.37	2017.80	0.487	0.186	174.5	75.7	107.2	3	Tok2017b
33077		±0.60	±0.08	±0.020	±0.003	±0.9	±1.2	±1.0		
06584−1300	HDS 969 AB	68.4	1979.1	0.164	0.795	38.3	217.6	93.7	5	New
07003−2207	FIN 334 Aa, Ab	217.5	2031.7	0.072	0.142	140.5	180.0	111.1	5	Doc2018e
07040−4337	TOK 390 Ca,Cb	4.623	2011.808	0.462	0.159	58.7	232.0	161.7	3	SaJ2011
34069		±0.040	±0.060	±0.014	±0.004	±21.0	±19.5	±8.1		
07116−7959	HDS 998	61.6	2021.5	0.095	0.117	34.7	53.6	40.5	5	New
07167+1609	HDS 1007	28.22	2014.51	0.319	0.228	345.4	126.5	81.9	3	New
35219		±0.29	±0.13	±0.011	±0.002	±0.4	±2.3	±0.6		
07336+1550	MCA 32	167	1993.71	0.879	0.428	97.1	269.1	83.6	4	Zir2008
36760		±27	±0.17	±0.033	±0.058	±0.4	±0.8	±0.7		
07427−3510	HDS 1091	120.6	2019.9	0.50	0.190	89.6	216.2	118.2	5	New
08342−0957	HDS 1226	55	2003.06	0.398	0.203	201.5	112.0	118.6	5	New
08444−4428	HDS 1256	12.695	2011.75	0.536	0.2902	140.5	60.3	146.9	4	New
42881		±0.068	±0.60	±0.091	±0.0359	±21.6	±29.6	±13.5		
08454−0013	A 2548	1100	1982.7	0.575	0.4974	179.2	230.1	114.9	5	New
08476−3124	HDS 1273	84.3	2020.38	0.572	0.272	236.5	90.0	99.4	5	New
08514−5047	HDS1281	25.8	2022.2	0.50	0.133	40.8	118.3	140.9	5	New
08571+1139	HDS1296	34.22	2003.33	0.836	0.580	219.2	131.2	105.6	3	New

Table 7
(Continued)

WDS *HIP*	Disc.	*P* (yr)	*T* (yr)	*e*	*a* (arcsec)	Ω (deg)	*ω* (deg)	*i* (deg)	Grade	Ref.[a]
43948		±0.59	±0.07	±0.006	±0.010	±0.4	±1.2	±0.4		
09024−6624	TOK 197	0.652	2015.593	0.041	0.0321	105.3	248.5	101.9	3	Tok2018i
44382		±0.001	±0.063	±0.038	±0.0013	±1.4	±34.2	±2.3		
09086−2550	TOK 357 BC	60	2070.0	0.20	0.299	177.0	39.6	66.8	5	New
09100−2845	B 179	80.35	2026.88	0.562	0.372	169.4	158.5	116.3	4	Doc2013c
45003		±0.84	±0.62	±0.025	±0.006	±1.1	±3.0	±1.3		
09293−4432	HDS 1360 Aa, Ab	79.5	2031.8	0.82	0.661	56.1	66.7	115.3	5	New
09442−2746	FIN 326	18.394	2020.96	0.504	0.107	175.3	138.9	127.0	2	Doc2013d
47758		±0.088	±0.17	±0.019	±0.002	±2.3	±4.1	±1.1		
09522+0807	A 2762	640	2092.6	0.60	1.603	131.1	17.3	105.8	5	New
09535+1657	CHR 219	54.0	2023.1	0.274	0.308	243.0	245.7	105.2	3	Hrt2012a
48504		±9.4	±1.7	±0.056	±0.020	±1.8	±23.8	±0.9		
10067+1754	HDS 1457	203	1989.2	0.649	0.684	109.1	298.9	126.2	5	MaB2016
10174−5354	CVN 16 Aa, Ab	5.327	2005.936	0.139	0.0952	129.0	96.5	15.3	2	Cvn2009
…		±0.021	±0.067	±0.013	±0.0023	±25.9	±25.7	±7.4		
10214−2616	HDS 1491	22.1	2022.75	0.287	0.113	262.8	0.0	180.0	5	New
10260+0256	A 2570	174	2023.5	0.83	0.245	122.9	329.4	114.3	5	Zir2014a
10264+2545	HDS 1500	85	1978.67	0.136	0.2130	150.8	317.6	65.2	5	New
10388−4245	FIN 338	80	2021.7	0.454	0.156	37.1	187.6	97.0	4	New
52112		fixed	±2.1	±0.041	±0.008	±0.8	±8.4	±2.0		
10419−7811	HDS 1530	39.07	2007.88	0.547	0.267	109.7	132.6	50.2	3	Tok2015c
52351		±0.67	±0.10	±0.008	±0.004	±1.5	±1.1	±0.7		
10455−2502	I 502 AB	256	2016.58	0.728	0.307	225.2	0.0	180.0	4	New
52615		±44	±0.22	±0.028	±0.028	±2.4	fixed	fixed		
10479−6416	HDS 1544	78	2003.8	0.319	0.224	96.3	175.0	127.5	5	New
11014−1204	HDS 1572	18.45	2013.69	0.682	0.172	142.4	133.6	97.4	3	Tok2015c
53879		±0.70	±0.03	±0.014	±0.003	±0.4	±1.4	±0.5		
11151−3929	SEE 128	95.0	1988.4	0.52	0.1353	165.1	72.9	46.4	3	New
54949		±4.5	±1.5	±0.06	±0.0161	±11.5	±13.9	±7.9		
11250−3200	CHR 242 Aa, Ab	13.47	2010.74	0.563	0.137	123.7	211.0	115.7	3	New
55714		±0.13	±0.14	±0.020	±0.002	±1.7	±4.7	±1.0		
11272−1604	HDS 1627 Aa, Ab	46.3	2003.5	0.358	0.222	89.9	165.0	119.5	4	New
55884		±3.2	±3.1	±0.031	±0.026	±4.7	±22.3	±7.0		
12096−6727	HDS 1716	72	2018.17	0.525	0.157	58.8	333.9	40.4	5	New
12250−0414	TOK 400	21.1	2018.77	0.61	0.211	96.9	182.0	125.9	5	New
12419−6444	HDS 1779	49	2019.86	0.675	0.124	206.7	128.2	118.1	4	New
61959		±15	±0.20	±0.10	±0.031	±3.1	±10.5	±10.5		
13081−7719	HDS 1839	17.01	2015.01	0.160	0.205	167.8	163.6	119.5	3	Tok2016e
64091		±0.36	±0.36	±0.026	±0.005	±1.5	±7.6	±1.2		
13417−2915	HDS 1922	88.4	2003.08	0.56	0.215	257.2	72.7	110.4	5	New
14094+1015	RAO 16	8.36	2018.88	0.98	0.104	114.0	66.0	114.4	5	New
14261−6536	HDS 2031	31.34	2009.26	0.50	0.183	245.1	133.3	104.2	5	New
14383−4954	FIN 371	51.6	2015.5	0.201	0.099	233.8	38.0	108.0	3	Tok2016e
71577		±3.3	±1.3	±0.027	±0.004	±1.3	±10.7	±1.1		
15481−2513	HDS 2226	31.1	2010.38	0.499	0.106	57.7	204.7	140.8	4	New
77399		±1.0	±0.60	±0.159	±0.008	±11.7	±20.1	±19.4		
15544−6131	HDS 2240	80	2020.57	0.83	0.188	183.4	0.0 6	0.0	5	New
16115+0943	FIN 354	61.1	1999.62	0.066	0.1281	263.8	91.6	90.2	3	Doc2013d
79337		±1.7	±0.71	±0.047	±0.0009	±0.3	±4.3	±0.6		
16115+0943	FIN 354	29.68	2000.91	0.742	0.0751	84.2	196.9	90.5	3	Doc2013d
79337		±0.22	±2.34	±0.124	±0.0039	±0.4	±27.0	±1.3		
16143−1025	RST 3936 AB	35	1999.92	0.818	0.173	263.6	160.6	109.7	5	New
16161−3037	I 1586	160	2050.85	0.200	0.361	0.1	261.2	137.9	5	New
16385−5728	TOK 51 Aa, Ab	25	2027.73	0.328	0.262	59.9	206.9	95.8	5	New
16514−2450	B 2397	69.4	2021.8	0.043	0.1534	22.4	76.6	120.5	3	New
82474		±3.4	±9.3	±0.034	±0.0024	±2.9	±52.0	±1.6		
17309−5621	FIN 257	700	2017.95	0.80	0.790	55.7	49.2	49.2	5	New
17430+0547	HDS 2506	21.07	2007.40	0.553	0.374	129.5	237.0	104.3	3	New
86707		±0.26	±0.03	±0.008	±0.004	±0.5	±1.2	±0.4		
17541−4821	B 1870	111.3	1999.76	0.487	0.153	110.7	151.6	126.9	3	New
87635		±6.7	±0.75	±0.024	±0.008	±3.5	±2.4	±2.3		
17577−2143	HDS 2530	59.9	1998.25	0.608	0.514	143.7	250.9	58.9	4	New
87925		±2.1	±0.56	±0.019	±0.013	±2.6	±2.3	±1.6		

Table 7
(Continued)

WDS *HIP*	Disc.	*P* (yr)	*T* (yr)	*e*	*a* (arcsec)	Ω (deg)	ω (deg)	*i* (deg)	Grade	Ref.[a]
18078+2606	CHR 67 Aa, Ab	35.53	2002.19	0.100	0.2954	144.8	82.7	77.1	2	Msn2001a
88818		±0.16	±0.26	fixed	±0.0026	±0.5	±2.4	±0.5		
18166−2033	MCA 51	119	2031.15	0.50	0.179	133.7	164.3	91.0	4	New
89567		±56	±8.12	fixed	±0.028	±0.6	±67.8	±0.6		
18448−3323	OL 20	490	2030.6	0.46	0.607	162.4	304.0	109.0	5	New
18520−5418	TOK 325 Aa, Ab	13.2	2017.12	0.314	0.106	110.7	308.3	47.3	3	Tok2017b
92592		±1.8	±0.21	±0.064	±0.004	±4.7	±13.0	±5.6		
19029−5413	I 1390	47.6	2009.434	0.666	0.185	73.8	220.7	58.6	3	Tok2015c
93524		±1.8	±0.047	±0.010	±0.004	±1.0	±1.5	±1.4		
19117−2604	RST 2094	245	2046.7	0.556	0.709	43.6	195.5	75.3	5	New
19194−0136	HDS 2734 Aa, Ab	36.83	2020.10	0.625	0.296	19.85	0	0	3	Tok2015c
94960		±0.29	±0.03	±0.012	±0.001	±0.40	fixed	fixed		
19240−5320	HDS 2751	20.61	2019.52	0.60	0.119	157.4	67.0	33.6	4	New
95360		±0.61	±0.13	fixed	±0.006	±12.8	±9.6	±5.2		
19407−0037	CHR 88 Aa, Ab	10.155	2012.847	0.463	0.0631	191.2	0.0	180.0	2	Tok2015c
96807		±0.033	±0.056	±0.010	±0.0006	±1.1	fixed	fixed		
19453−6823	TOK 425 Ba, Bb	4.12	2017.09	0.80	0.0504	136.6	202.0	124.5	4	New
97196		±0.24	±0.12	fixed	±0.0053	±12.8	±24.6	±8.3		
19531−1436	CHR 90	343.2	1998.85	0.716	0.678	3.3	73.5	126.5	5	Cve2010b
21206+1310	HDS 3038	78.2	2012.84	0.25	0.231	126.1	274.3	91.1	5	New
21330+2408	HDS 3065 Aa, Ab	67.3	2025.0	0.63	0.466	75.8	30.7	101.3	5	New
21522+0538	JOD 23 AB	9.39	2019.48	0.417	0.142	161.9	0.0	0.0	4	New
107948		±0.13	±0.04	±0.011	±0.002	±1.3	fixed	fixed		
22003−2330	I 674	301	2007.87	0.852	0.500	69.4	44.5	59.7	3	New
…		±57	±0.11	±0.019	±0.059	±1.2	±1.8	±1.1		
22061−0521	TOK 373	13.1	2013.53	0.366	0.182	45.6	352.3	96.4	4	
109110		fixed	±0.22	±0.021	±0.003	±0.7	±8.0	±1.1		New
22083+2409	HDS 3145	10.641	1997.760	0.516	0.0951	62.0	301.9	149.4	1	Bag2007b
109281		±0.044	±0.048	±0.013	±0.0012	±4.5	±4.3	±2.2		
22116−3428	CHR 230 Aa, Ab	43.4	2010.29	0.831	0.104	130.7	134.1	75.1	3	Tok2016e
109561		±2.4	±0.37	±0.023	±0.0010	±2.0	±6.4	±2.1		
22126−1802	HDS 3153	35.7	2022.09	0.78	0.177	57.2	49.1	124.2	5	New
22259−7501	TOK 434 Ba, Bb	11.0	2022.21	0.25	0.254	235.0	270.0	87.3	5	New
22357−2808	HDS 3208 Aa, Ab	19.13	2021.76	0.51	0.174	133.6	209.3	70.9	4	New
111520		±0.95	±1.32	±0.11	±0.016	±3.3	±12.5	±4.8		
22376+2400	HDS 3212	31.22	2027.60	0.357	0.110	133.6	145.7	31.1	4	New
111694		±0.58	±1.01	±0.021	±0.003	±9.6	±14.6	±7.8		
22493+1517	HDS 3241	92.5	2005.6	0.703	0.235	144.9	348.7	52.6	3	Doc2013f
112695		±12.9	±0.1	±0.028	±0.022	±1.6	±1.6	±1.6		
23270−1515	HU 297	92.6	1983.5	0.90	0.374	142.5	48.6	111.5	4	New
115742		±2.9	±1.8	fixed	±0.067	±3.2	±11.3	±7.8		
23286−3821	HDS 3342	46.6	2014.9	0.368	0.119	125.3	155.6	122.8	5	New
23350+0136	MEL 9 BC	31.81	1998.66	0.0	0.437	10.5	0.0	84.2	4	New
116384		±0.18	±0.06	fixed	±0.005	±0.6	fixed	±0.5		
23597−4405	WSI 140	11.77	2001.98	0.394	0.217	93.4	0.0	0.0	3	TSN2017
…		±0.39	±0.39	±0.007	±0.004	±2.6	fixed	fixed		

Note.
[a] References to VB6 are provided at http://ad.usno.navy.mil/wds/orb6/wdsref.txt.

hidden and instead leaves an impression that the object is neglected by observers. Here we present a list of likely spurious pairs, hoping to clean the WDS catalog and to reduce the waste of effort for their observation. In a sense, this is a necessary complement of new discoveries presented above.

Two enigmatic cases of "ghost" visual pairs with multiple spurious historic measures were presented by Tokovinin (2012); other likely spurious visual binaries are suggested here, namely several pairs by van den Bos (discoverer code B). An intriguing case is WDS J03244−1539 (A 2909AB), for which a grade 3 orbit with $P = 11.35$ yr was computed. This object was visited at SOAR 13 times between 2007 and 2018 and resolved only once in 2013.74; the nonresolutions contradict the orbit, and we believe that this star is single (it has a constant RV). Other observing techniques also contributed their share of spurious pairs, for various reasons. In speckle interferometry, doubling or elongation can be caused by telescope vibration, optical ghosts (see Tokovinin et al. 2018), or poorly corrected atmospheric dispersion. A number of CHARA pairs were withdrawn as false resolutions by McAlister et al. (1993); several more are spotted here. Similarly, some resolutions at SOAR (discoverer code TOK) are likely spurious, as revealed by subsequent observations. Lunar occultations have supplied quite a few false double stars,

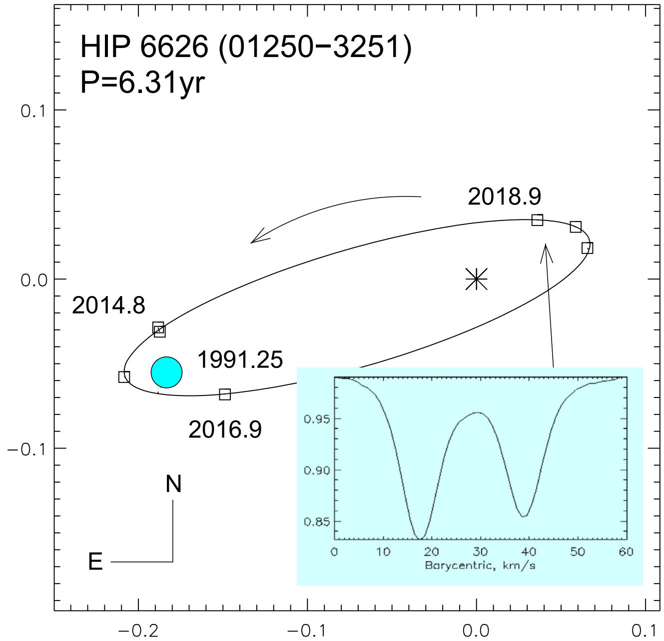

Figure 7. Orbit of HIP 6626 (HDS 184, WDS J01250-3251). The primary component is located at the coordinate origin, with scale in arcseconds. The ellipse marks the trajectory. The original *Hipparcos* discovery is marked by the blue circle, the SOAR measures from 2014.8 to 2018.9 by squares. The insert shows double lines observed on 2018.916, shortly after the periastron passage.

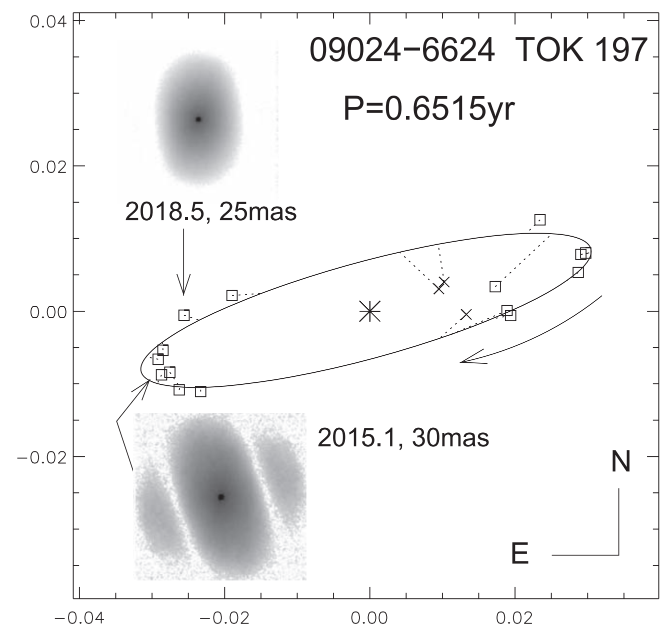

Figure 8. Orbit of α Vol (WDS J09024-6624). The inserts show power spectra recorded in 2015.1 near maximum separation and in 2018.5 at separation of 25 mas. Crosses denote nonresolutions.

and many *Tycho* pairs with small separations are spurious as well (Tokovinin et al. 2018). Other reasons of spurious discoveries are optical pairs with fast relative motion and pointing wrong stars.

It is almost impossible to prove with certainty that a given star is not double; our conclusions on the spurious nature of some pairs are based on the available evidence. When a pair discovered visually is repeatedly unresolved with a more powerful technique such as speckle, it is very likely spurious. Estimation of the orbital period based on angular separation and distance from the Sun helps to reject the pair when its speckle coverage is of comparable duration or when the period is very long, as the usual hypothesis that the binary became temporarily too close can be dropped. A number of spurious subsystems can be rejected because the outer binaries were repeatedly measured by speckle without resolving the subsystem, as, for example, WDS J15462−280, one of our calibrators; its subsystem CHR 50 is definitely spurious (Tokovinin 2012).

Table 8 presents the list of candidate spurious double stars observed at SOAR. Its first two columns link the pair to the WDS catalog (Mason et al. 2001). Column (3) describes the resolution by giving the separation in arcseconds, measurement technique (Vis, visual; Sp, speckle; HIP, *Hipparcos*; Tyc, *Tycho*; Occ, lunar occultations), and the years when the pair was resolved. The last column gives the years of nonresolutions at SOAR and additional hints coded by letters. DR2 indicates nonresolution by *Gaia* (resolved binaries do not have parallaxes in DR2). Many objects are located at large distances, and their separations, if real, imply periods of >100 years (code L). Similarly, the code S means that the period of nonresolution is comparable to the short estimated binary period; in some cases the spectroscopic orbit provides strong evidence against the existence of close visual binaries. False resolutions at SOAR are explained, mostly, by the effect of vibration (see Figure 6 of Tokovinin 2018) that was not fully appreciated during the first years of HRCam operation (code Vib) and by optical ghosts (code OG). Although some observations presented here are still affected by vibration, this is now recognized and compensated for by the use of reference stars with similar artifacts. Several objects in Table 8 are unresolved subsystems in visual triple stars, while their successfully measured pairs are found in Table 2.

The WDS J07185−5724 (RST 244 Ba,Bb) is a special case (Figure 9). The pair Ba,Bb in a visual quadruple system HIP 35374 (Aa,Ab is a $0\farcs4$ binary) was discovered with the HRcam at SOAR at $0\farcs9$ separation in 2010 and measured several times since. It was observed here with the full field to show that the companion Bb corresponds to the peak produced by correlation between B and Ab; it is aliased and appears at the wrong position when the data cubes with the $6\farcs2$ field are recorded. Consequently, the pair Ba,Bb does not exist, and this system is only a triple.

4. Summary

Continued monitoring of close visual binaries at SOAR makes a substantial contribution to the definition of their orbits, especially for tight and nearby pairs with short periods like HIP 6626 (Figure 7). Good-quality visual orbits coupled to precise parallaxes from *Gaia* will vastly extend our knowledge of stellar masses. Moreover, visual orbits are needed in different astrophysical contexts. To give an example, our orbit of the exoplanet host HIP 49522 (10067+1754) with $P = 203$ yr is still poorly constrained, but the premature 51-year orbit proposed by Ma et al. (2016) is certainly refuted by our measurements, resolving the apparent conflict with the planetary orbits discussed in the above paper.

The SOAR speckle program resulted in the discovery of many new close binaries and subsystems. This list is extended here by the 35 new subsystems in visual multiples, newly

Table 8
Spurious Pairs

WDS	Disc.	Resolved	Unresolved[a]
00023−2943	B 631	3″ Vis 1925-27	2018, DR2
00028−2353	B 632	0.″2 Vis 1926-31	2018, L
02098−4052	TOK 427	0.″4 Sp 2014	Vib
03244−1539	A 2909AB	0.″1 Vis 1918-2013	2007–18, S
03590−0056	HEI 215AB	1.″8 Vis 1973-97	2018, L
06273+1453	CHR 251	0.″05 Sp 1995	2016–18, L
06448−0424	HDS 937	0.″5 HIP	2016–18, L
06461−2045	I 760	1.″2 Vis 1910	2018, DR2
06523−0510	WSI 125Bab	0.″1 Sp. 2010	2014–17, DR2
06533−1528	HDS 954	0.″6 HIP	2018, L
06585−2406	HDS 971	1.″0 HIP	2015-18, L
07185−5724	RST 244Bab	0.″9 Sp 2010-16	Alias
07431+0011	B 2526AB	0.″1 Vis 1936-62	1976–2018
07501−2815	HDS1113	0.″4 HIP	2015-18, L
08095−4720	WSI 55Bab	0.″1 Sp 2006-09	2014–18, L
08107−7430	B 1981AB	0.″2 Vis 1936	2018, DR2
09128−6055	CHR 144Aab	0.″02 Sp 1989	1990–2018, S
10311−2411	CHR 132Aab	0.″1 Sp 1987-89	2010–18, S
10560−6024	HDS1561	0.″3 HIP	2018, L
11383−6039	HDS1649	0.″2 HIP	2018, L
12492−6040	HDS1797	0.″2 HIP	2018, L
15037−5423	TDS9389	2.″2 Tyc	2018, DR2
15066−3055	HDS2128AB	0.″4 HIP	2016–18, L
15168−1302	CHR 44	0.″2 Sp 1983–86	2012–18
15384−1955	CHR 48	0.″3 Sp 1983	2012–18
15470−3635	HDS2223	0.″13 HIP	2008–18, L
15578−4100	SEE 252AB	0.″4 Vis 1897	2008–18, L
16072−2531	OCC 150	0.″1 Occ 1931	2018, L
16083−2537	OCC 148	0.″1 Occ 1931	2018, L
16141−1812	OCC 519	0.″35 Occ 1977	2018, L
16406+0413	CHR 56Aab	0.″14 Sp 1985–88	2008–18, S
16407−6233	B 1816	0.″3 Vis 1939	2018, L
16459−3953	HDS2380	0.″13 HIP	2008–18, L
17098−1031	TOK 414	0.″04 Sp 2014	2014–18, S
17146+1423	CHR 139Aab	0.″2 Sp 1986–91	2009–18
17341−0303	TOK 417	0.″1 Sp 2014	2015–18, OG
18068+0853	TOK 696Aab	0.″03 Sp 2015	2015–18, Vib
18070+3034	SCA 170Aab	0.″2 2000-05	1989–2018, S
18112−1951	TOK 57Aab	0.″05 Sp 2008–09	2011–18, Vib
18232−2825	HDS2601	0.″17 HIP	2017–18, L
18267−3024	TOK 421	0.″07 Sp 2014	2014–18, Vib
18272+0012	STF2316Aab	0.″2 Sp 1951–2009	2008–18, S
19094+1014	CHR 140	0.″25 Sp 1985	2015–18, L
19294−0703	TOK 4Aa, Ab	0.″05 Sp 2009	2008–18, Vib
19488−4931	HDS2818	0.″17 HIP	2008–18, L
19503+0754	CHR 89	0.″06 Sp 1985–86	2017–18, L
19510−0252	TOK 213Aab	0.″1 Sp 2014	2014–18, OG
20254−2840	CHR 97	0.″1 Sp 1983	2013–18, S
20449+1219	B 2910Aab	0.″2 Vis 1937	1976–2018, S
23315−2857	B 602	0.″2 Vis 1925–32	2008–18, L
23388−2816	B 608	0.″2 Vis 1925–29	2008–18
23444−7029	WSI 94	0.″05 Sp 2008	2012–18, Vib
23598+0640	BAG 31Aab	0.″2 Sp 2001	2015–18, S

Note.
[a] Additional indications of the spurious nature of visual pairs: DR2, parallax provided by *Gaia* DR2; OG, optical ghost (Tokovinin et al. 2018); L, long estimated period; S, short estimated period or spectroscopic coverage; Vib, artifact caused by telescope vibration.

resolved *Hipparcos* stars, and tight PMS binaries in Orion OB1. SOAR speckle observations of PMS stars in various nearby star-forming regions are a key part of our multiplicity studies in young stellar populations, probing the separation regime ∼30–1000 au at ∼400 pc. Understanding the formation of stellar systems requires comprehensive multiplicity census of PMS stars across regions with differing conditions.

During 2018, the core program on visual multiples has been supplemented by various binary surveys; high-resolution screening of *TESS* exoplanet candidates has started as well. These programs will be continued and their results will be published in forthcoming papers.

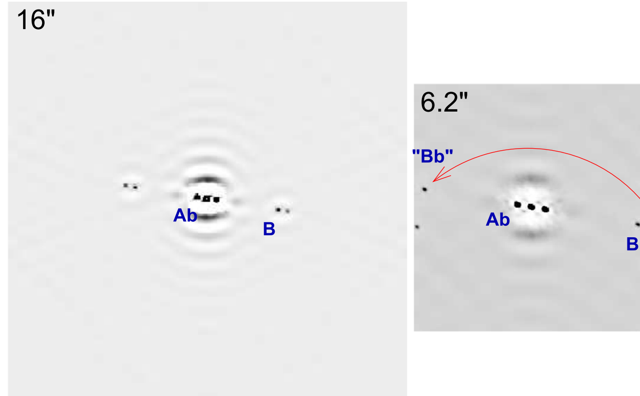

Figure 9. Triple system 07185−5724. The left panel shows ACF of the data cube recorded in 2018.2 with the full field; the peaks corresponding to the companions Ab at 0.″4 and B at 2.″9 are indicated. In the right panel, the ACF in the 6.″2 field is shown. The peak corresponding to the correlation between Ab and B (red circle) falls outside the field and is aliased (reflected) to a different position (red arrow), creating an illusion of another companion Bb.

The authors thank the SOAR operators for efficient support of this program, and the SOAR director J. Elias for allocating some technical time. A through checking by the anonymous referee has helped to improve the presentation and to correct some errors.

This work is based in part on observations carried out under CNTAC program CN2018A-2. R.A.M. acknowledges support from the Chilean Centro de Excelencia en Astrofísica y Tecnologías Afines (CATA) BASAL AFB-170002, and FONDECYT/CONICYT grant # 1190038.

This work used the SIMBAD service operated by Centre des Données Stellaires (Strasbourg, France), bibliographic references from the Astrophysics Data System maintained by SAO/NASA, and the Washington Double Star Catalog maintained at USNO. This work has made use of data from the European Space Agency (ESA) mission *Gaia* (https://www.cosmos.esa.int/gaia processed by the *Gaia* Data Processing and Analysis Consortium (DPAC, https://www.cosmos.esa.int/web/gaia/dpac/consortium Funding for the DPAC has been provided by national institutions, in particular the institutions participating in the *Gaia* Multilateral Agreement.

Facility: SOAR.

ORCID iDs

Andrei Tokovinin https://orcid.org/0000-0002-2084-0782
Brian D. Mason https://orcid.org/0000-0003-4824-0938
Elliott P. Horch https://orcid.org/0000-0003-2159-1463
Cesar Briceño https://orcid.org/0000-0001-7124-4094

References

Briceño, C., Calvet, N., Hernández, J., et al. 2019, AJ, 157, 85
Briceño, C., & Tokovinin, A. 2017, AJ, 154, 195

Elliott, P., Huélamo, N., Bouy, H., et al. 2015, A&A, 580, 88
Gaia Collaboration, Brown, A. G. D., Vallenari, A., et al. 2018, A&A, 595, A2
Hartkopf, W. I., Mason, B. D., & Worley, C. E. 2001, AJ, 122, 3472
Hartkopf, W. I., Tokovinin, A., & Mason, B. D. 2012, AJ, 143, 42
Holmberg, J., Nordstrom, B., & Andersen, J. 2009, A&A, 501, 941
Horch, E. I., Tokovinin, A., Weiss, S. A., et al. 2019, AJ, 157, 56
Horch, E. P., Casetti-Dinescu, D. I., Camarata, M. A., et al. 2017, AJ, 153, 212
Horch, E. P., van Belle, G. T., Davidson, J. W., Jr., et al. 2015, AJ, 150, 151
Ma, B., Ge, J., Wolszczan, A., et al. 2016, AJ, 152, 112
Mason, B. D., Wycoff, G. L., Hartkopf, W. I., et al. 2001, AJ, 122, 3466, (WDS)
Mason, B. D., Hartkopf, W. I., Miles, K. N., et al. 2018, AJ, 155, 215
McAlister, H. A., Mason, B. D., Hartkopf, W. I., & Shara, M. M. 1993, AJ, 106, 1639
Mendez, R. A., Claveria, R. M., Orchard, M. E., & Silva, J. F. 2017, AJ, 154, 187
Perryman, M. A. C., Lindegren, L., Kovalevsky, J., et al. 1997, A&A, 323L, 49
Tokovinin, A. 2012, AJ, 144, 56
Tokovinin, A. 2016a, AJ, 152, 138
Tokovinin, A. 2016b, ORBIT: IDL Software for Visual, Spectroscopic, and Combined Orbits, Zenodo, doi:10.2581/zenodo.61119
Tokovinin, A. 2018a, PASP, 130, 5002
Tokovinin, A. 2018b, ApJS, 235, 6
Tokovinin, A. 2018c, AJ, 155, 160
Tokovinin, A., & Briceño, C. 2018, AJ, 156, 138
Tokovinin, A., Cantarutti, R., Tighe, R., et al. 2010a, PASP, 122, 1483
Tokovinin, A., Cantarutti, R., Tighe, R., et al. 2016a, PASP, 128, 125003
Tokovinin, A., Mason, B. D., & Hartkopf, W. I. 2010b, AJ, 139, 743, (TMH10)
Tokovinin, A., Mason, B. D., & Hartkopf, W. I. 2014, AJ, 147, 123
Tokovinin, A., Mason, B. D., Hartkopf, W. I., et al. 2015, AJ, 150, 50, (SOAR14)
Tokovinin, A., Mason, B. D., Hartkopf, W. I., et al. 2016b, AJ, 152, 116
Tokovinin, A., Mason, B. D., Hartkopf, W. I., et al. 2018, AJ, 155, 235